POLITECNICO DI TORINO
Repository ISTITUZIONALE

Automatic Segmentation of Multicellular Tumour Spheroids Images During Growing

Original
Automatic Segmentation of Multicellular Tumour Spheroids Images During Growing / Introvaia, A., Muccio, S., Bezze, A., Mattu, C., Balestra, G.. - ELETTRONICO. - 321:(2024), pp. 230-234. (European Federation for Medical Informatics Special Topic Conference (EFMI STC) 2024 - Collaboration across Disciplines for the Health of People, Animals and Ecosystems Timisoara (RO) 27 to 29 November 2024) [10.3233/shti241098].

Availability:
This version is available at: 11583/2994745 since: 2024-11-24T19:11:44Z

Publisher:
IOS Press

Published
DOI:10.3233/shti241098

Terms of use:

This article is made available under terms and conditions as specified in the corresponding bibliographic description in the repository

Publisher copyright

(Article begins on next page)

17 November 2026

Available online at www.sciencedirect.com

ScienceDirect

Procedia Structural Integrity 13 (2018) 596–600

Structural Integrity Procedia

www.elsevier.com/locate/procedia

ECF22 - Loading and Environmental effects on Structural Integrity

Brazilian disk tests: Circular holes and size effects

A.R. Torabi [a], S. Etesam [a], A. Sapora [b]*, P. Cornetti [b]

[a]*Fracture Research Laboratory, Faculty of New Sciences and Technologies, University of Tehran, P.O. Box 14395-1561, Tehran, Iran*
[b]*Department of Structural, Geotechnical and Building Engineering, Politecnico di Torino, 10129 Torino, Italy*

Abstract

Size effects related to circular notched samples imply that the strength of the structure decreases as the hole radius increases. In this framework, Brazilian disk tests are carried out on brittle samples containing a circular hole. By considering two different polymers, namely Polymethyl-methacrylate (PMMA) and General-purpose Polystyrene (GPPS), respectively, five different notch radii were machined and tested for each material, keeping low the hole to disk diameter ratio in order to reproduce an infinite geometry. Under this assumption, analytical relationship for the stress field and the stress intensity factor can be implemented without loss of accuracy. The coupled finite fracture mechanics (FFM) is then applied to catch the recorded failure stresses, allowing a complete description of the experimental size effects. On the contrary, the smallest radius leads to a locally negative geometry, opening the discussion on the stability of crack propagation in circularly notched plates under generic biaxial loadings.

© 2018 The Authors. Published by Elsevier B.V.
Peer-review under responsibility of the ECF22 organizers.

Keywords: Size effects; Circular holes; FFM; Negative geometries.

1. Introduction

After more than one century since the well-known work by Kirsch (1898) on the stress field around a circular hole subjected to remote tensile load, the problem of the related size effects has recently come back to the scientific attention (Furtado et al. 2017, Torabi et al. 2017, Sapora et al. 2018). Indeed, some relevant discrepancies have been detected between experimental results and the theoretical predictions by well-established failure criteria based on a critical distance (Li and Zhang 2006). The whole question is here reconsidered both from an experimental and a theoretical point of view. As concerns the former aspect, Brazilian disk (BD) tests on notched samples are carried out by considering two different polymeric materials, PMMA and GPPS. Five different circular hole sizes are machined for each material specimen keeping small the hole to disk radius ratio. As regards the latter aspect, the coupled stress and

* Corresponding author. Tel.: +39-090-4819, Fax: +39-090-4890
E-mail address: alberto.sapora@polito.it

2452-3216 © 2018 The Authors. Published by Elsevier B.V.
Peer-review under responsibility of the ECF22 organizers.
10.1016/j.prostr.2018.12.098

energy criterion in the framework of Finite Fracture Mechanics (FFM, Cornetti et al. 2006) is implemented. FFM predictions are obtained by referring to an infinite geometry and exploiting the analytical relationships for the stress field (Kirsch 1898) and the stress intensity factor (Tada et al. 2000) available in the Literature. The criterion involves just two material properties, the material tensile strength σ_u and the fracture toughness K_{Ic}, and it reveals to be an efficient tool to describe the size effects for the geometry under investigation. Finally, the analysis provides some issues on the stability investigation of crack initiation in biaxial plates, which are briefly discussed starting from the works by Mantič (2009) and Weißgraeber et al. (2016).

2. Experimental tests

For the experimental campaign, two different brittle polymers were taken into account: PMMA and GPPS, respectively. The tensile strength and the fracture toughness for the two materials are: σ_u = 78 MPa and K_{Ic} = 1.75 MPa√m for PMMA, σ_u = 40 MPa and K_{Ic} = 0.9 MPa√m for GPPS. Interestingly, the value of $l_{ch} = (K_{Ic} / \sigma_u)^2$ is nearly the same in both cases, and equal to 0.5 mm.

Experimental tests were carried out in the Fracture Research Laboratory of the University of Tehran on notched BD. By referring to the sample geometry depicted in Fig. 1a, the diameter $2R_0$ was fixed equal to 80 mm, and the thickness t to 10 mm for PMMA samples, and to 8 mm for GPPS samples. In both cases, t was large enough to achieve plane strain conditions, since $t \geq 2.5\ l_{ch}$. Five different hole sizes were considered with the following dimensions: $2R$ = 0.5, 1, 2, 4, and 8 mm. The test speed was set equal to 0.5 mm/min in order to prevent possible instabilities in the compression tests. The experimental fracture was of brittle character (Fig.1 b,c), but increasing non-linearities were observed in the force-displacement curves for decreasing hole sizes (Torabi et al. 2018).

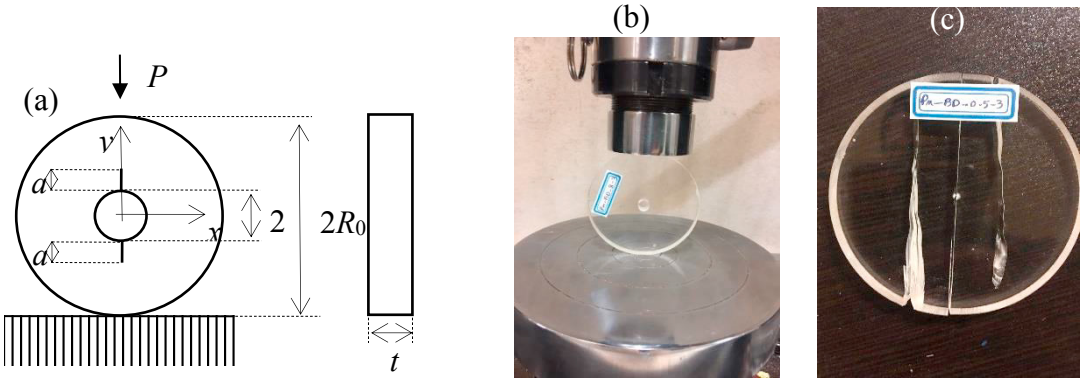

Fig. 1. (a) Geometry under investigation; (b) experimental test on a PMMA notched sample (R=8mm); (c) broken PMMA sample (R=0.5 mm).

The recorded failure stresses are presented in Table 1, together with the average value $\bar{\sigma}_f$ of the related failure stress, rising from:

$$\sigma = \frac{P}{\pi R_0 t} \tag{1}$$

3. FFM criterion

With respect to the frame of reference xy depicted in Fig. 1a, the coupled FFM criterion (Cornetti et al. 2006, Sapora et al. 2015), can be expressed as:

$$\begin{cases} \dfrac{1}{\Delta}\displaystyle\int_0^{\Delta} K_I^2(a)da \geq K_{Ic}^2 \\ \dfrac{1}{\Delta}\displaystyle\int_R^{R+\Delta} \sigma_x(y)dy \geq \sigma_u \end{cases} \tag{2}$$

where K_I is the stress intensity factor (SIF) related to a crack of length a stemming from the notch tip, and σ_x is the tensile stress along the axial loading (Fig. 1). For positive geometries the strain energy release rate function (and thus the SIF K_I) is monotonically increasing with a: at incipient failure Eq. (2) will turn into a system of two equations in two unknowns: critical crack advance Δ_c and nominal failure stress σ_f, which is implicitly embedded in functions K_I and σ_x.

Table 1. Experimental failure loads and average failure stresses.

PMMA			GPPS		
$2R$ (mm)	P_f (N)	$\bar{\sigma}_f$ (MPa)	$2R$ (mm)	P_f (N)	$\bar{\sigma}_f$ (MPa)
0.5	37150		0.5	15930	
0.5	33810	28.377	0.5	15280	15.020
0.5	36020		0.5	14090	
1	28800		1	12260	
1	26230	22.003	1	11970	11.986
1	27920		1	11920	
2	21830		2	9950	
2	24700	18.469	2	9130	9.3106
2	23100		2	9000	
4	20250		4	8070	
4	19936	15.453	4	7645	7.7190
4	18074		4	7565	
8	14414		8	6525	
8	16168	12.205	8	6220	6.2767
8	15432		8	6185	

For sufficiently small hole radii, the SIF function related to a crack of length a stemming from the notch can be approximated with the one valid for a circular hole in an infinite plate, where

$$K_I(a) = \sigma\sqrt{\pi a}\, F(s) \tag{3}$$

with

$$s = \frac{a}{a+R} \tag{4}$$

The shape function F related to the symmetric crack propagation (Fig. 1a) can be written as (Tada et al. 2000):

$$F(s) = (1-\lambda)\left\{0.5\,(3-s)\,[1+1.243(1-s)^3]\right\} + \lambda\left\{1+(1-s)\,[0.5+0.743(1-s)^2]\right\} \tag{5}$$

where $\lambda = -3$ according to the present geometry.

Furthermore, Kirsch solution (note that in the centre of a plain specimen the stress is equal to -3σ in the y-direction) yields the approximate solution for the stress field function:

$$\sigma_x(y) = \frac{\sigma}{2}\left(2 - 2\frac{R^2}{y^2} + 12\frac{R^4}{y^4}\right) \tag{6}$$

Equation (6) provides ideally a stress concentration factor $\sigma_x(y=R)/\sigma = 6$, meaning that the maximum stress is 6 times higher than the nominal one. Indeed, the accuracy of Eqs. (3) and (6) could be improved for not negligible R/R_0 ratios by taking the following multiplying factor into account:

$$F_{corr} = 1 + \frac{19}{3}\left(\frac{R}{R_0}\right)^2 \tag{7}$$

The FFM criterion (1) can now be implemented by means of Eqs. (3), (6) and (7). By introducing the function f related to the integration of the stress field (6) and the function g related to the integration of the SIF squared (3), some analytical manipulations allow to write the FFM system at failure as $\tilde{\Delta}_c = \Delta_c / R$:

$$\begin{cases} f\left(\tilde{\Delta}_c\right) - \sqrt{\Delta_c \, g\left(\tilde{\Delta}_c\right)/l_{ch}} = 0 \\ \dfrac{\sigma_f}{\sigma_u} = \dfrac{\tilde{\Delta}_c}{f\left(\tilde{\Delta}_c\right)} \end{cases} \tag{8}$$

FFM predictions on both PMMA and GPPS experimental data are reported in Fig. 2. The size effects are well-caught by FFM, and the trend of theoretical predictions is similar for both materials. As can be seen, FFM results are accurate for $2R$=8, 4, 2, and 1 mm, with discrepancies below 13%. On the other hand, the accuracy decreases (discrepancies above 20%) for the smallest hole, i.e., $2R$=0.5 mm. This behavior is imputable to some nonlinear phenomena (detected in the stress-displacement curves) related to the high failure load and the particular (compressive) loading conditions.

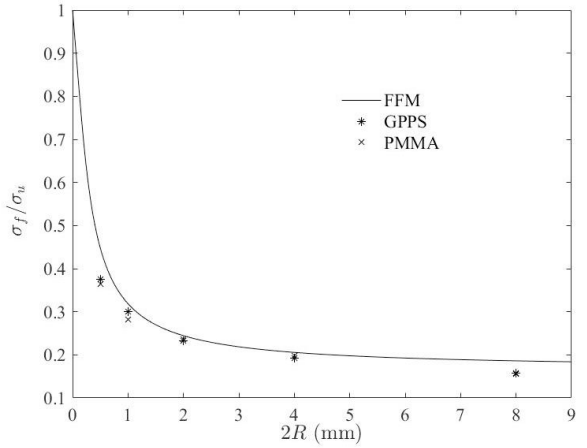

Fig. 2. Dimensionless failure stress vs. hole diameter: FFM predictions and average experimental data (circles).

4. Crack stability

The case analyzed in the previous section, as already outlined, is equivalent, from a mechanical point of view, to a plate under biaxial loading (Fig. 3 with λ=–3). In this case, the function K_I is no longer monotonically increasing, as its average value $\overline{K}$, which corresponds to the former equation in (2). Indeed, $\overline{K}$ is increasing only for $\tilde{\Delta} < \tilde{\Delta}^* \vee \tilde{\Delta} > \tilde{\Delta}^{**}$. If $\tilde{\Delta}^* \le \tilde{\Delta} < \tilde{\Delta}^{**}$ (to which corresponds $\hat{R}^{**} \le \hat{R} = R/l_{ch} < \hat{R}^*$), the FFM criterion cannot be longer described by system (1), but it has to be replaced by the condition (Mantic 2009):

$$\overline{K}(\tilde{\Delta}^*) = \sqrt{\frac{1}{\tilde{\Delta}^*}\int_0^{\tilde{\Delta}^*} K_I^2(\tilde{a})\,d\tilde{a}} = K_{Ic} \tag{9}$$

This geometry was referred to as locally negative/globally positive by Weißgraeber et al. (2016).

Of course the values of $\tilde{\Delta}^*$, $\hat{R}^*$ and $\tilde{\Delta}^{**}$, $\hat{R}^{**}$ depend on the parameter λ: as it decreases, $\tilde{\Delta}^*$ tend to 0.31 and $\hat{R}^*$ to 1.44, whereas $\tilde{\Delta}^{**}$ diverges and $\hat{R}^{**}$ tends to zero. In other words, as $\lambda \to -\infty$ the distance between $\hat{R}^{**}$ and $\hat{R}^*$ increases (Fig. 3), and the limits of compressive loading are qualitatively recovered. As concerns the data presented in Table 1, the smallest hole corresponds to $\hat{R}$ =0.5, which is comprised between 0.24 and 0.68 for λ=–3 (Fig. 3). Thus, FFM predictions should have been obtained by means of Eq. (9). On the other hand, this aspect was disregarded in the theoretical analysis (Fig. 2) and Eq. (8) was implemented instead. The committed error is not significant in terms of failure stress, but a relevant deviation could have been observed on critical crack advance, which unfortunately was not measured experimentally. In order to stress this behavior, it would be interesting to carry out similar tests by reducing $\hat{R}$: since machining smaller hole diameters could result in a difficult task, this means considering a material less brittle (increasing thus l_{ch}) than GPPS or PMMA .

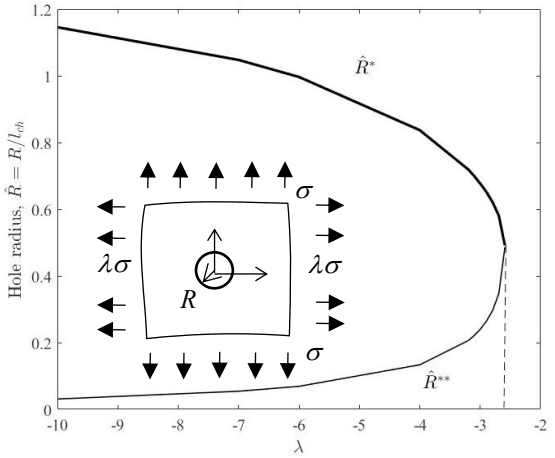

Fig. 3. Circularly notched plates under biaxial loading: $\hat{R}^*$ and $\hat{R}^{**}$ values vs. loading parameter, λ.

5. Conclusions

In the present work size effects related to circular notched samples are investigated both experimentally, by testing PMMA and GPPS notched samples, and theoretically by means of FFM. Actually, FFM predictions are accurate but for the smallest hole sizes, where the failure stress is overestimated: this discrepancy (more than 20%) is imputable to some nonlinear phenomena (detected in the stress-displacement curves) related to the high failure load and the particular (compressive) loading conditions. The investigation of nonlinearities goes beyond the scope of the paper, but some works are in progress following the study by Leguillon and Yoshibash (2017).

Finally, in the more general framework of plates under biaxial loading conditions, it has been shown that the loading parameter λ and the dimensionless hole radius govern the FFM stability of the crack onset.

References

Cornetti, P., Pugno, N., Carpinteri, A., Taylor, D. (2006). Finite fracture mechanics: a coupled stress and energy failure criterion. Engineering Fracture Mechanics 73, 2021–33.

Furtado, C., Arteiro, A., Bessa, M.A., Wardle, B.L., Camanho, P.P. , 2017. Prediction of size effects in open-hole laminates using only the Young's modulus, the strength, and the R-curve of the 0° ply, Composites Part A: Applied Science and Manufacturing 101, 306-317.

Kirsch, E.G. 1898. Die Theorie der Elastizität und die Bedürfnisse der Festigkeitslehre. Zeitschrift des Vereines deutscher Ingenieure 42, 797-807.

Leguillon, D., Yosibash, Z. 2017. Failure initiation at V-notch tips in quasi-brittle materials. International Journal of Solids Structures 122-3, 1-13.

Li, J, Zhang, X., 2006. A criterion study for non-singular stress concentrations in brittle or quasi-brittle materials. Engineering Fracture Mechanics 73, 505-523.

Mantič, V. 2009. Interface crack onset at a circular cylindrical inclusion under a remote transverse tension. Application of a coupled stress and energy criterion. International Journal of Solids and Structures 46, 287-1304.

Sapora, A., Cornetti, P., Carpinteri, A., Firrao, D. 2015. An improved Finite Fracture Mechanics approach to blunt V-notch brittle fracture mechanics: Experimental verification on ceramic, metallic, and plastic materials. Theoretical and Applied Fracture Mechanics 78, 20–24.

Sapora, A., Torabi, A.R., Etesam, S., Cornetti, P., 2018. Finite Fracture Mechanics crack initiation from a circular hole, Fatigue Fract Eng Mater Struct, 1–10. https://doi.org/10.1111/ffe.12801.

Tada, H., Paris, P., Irwin, G., 2000. The Stress Analysis of Cracks Handbook. Third Edition, Paris Productions Incorporated, St Louis, MO, USA.

Torabi, A.R., Etesam, S., Sapora, A., Cornetti, P., 2017. Size effects on brittle fracture of Brazilian disk samples containing a circular hole, Engineering Fracture Mechanics 186, 496–503.

Weißgraeber, P., Hell, S., Becker, W., 2016. Crack nucleation in negative geometries, Engineering Fracture Mechanics 168, 93–104.